Spatial variability in mass loss of glaciers in the Everest region, central Himalaya, between 2000 and 2015

Owen King[1], Duncan J. Quincey[1], Jonathan L. Carrivick[1], Ann V. Rowan[2]

[1]School of Geography and water@leeds, University of Leeds, Leeds, LS2 9JT, UK.

[2]Department of Geography, University of Sheffield, Sheffield, S10 2TN, UK.

Correspondence to: gy08ok@leeds.ac.uk

Abstract. The mass balance of the majority of Himalayan glaciers is currently negative, and has been for several decades. Region wide averaging of mass change estimates has masked any catchment or glacier scale variability in glacier recession, thus the role of a number of glaciological processes in glacier wastage remains poorly understood. In this study, we quantify mass loss rates over the period 2000-2015 for 32 glaciers in different catchments across the Everest region, and specifically examine the role of 7 proglacial, and 2 supraglacial glacial lakes in glacier mass loss. We then assess how future ice loss is likely to differ depending on glacier hypsometry. Spatially variable ice loss is observed within and between the Dudh Koshi and Tama Koshi catchments and glaciers that flow onto the Tibetan Plateau. The mean mass balance of the 32 glaciers in our sample was –0.54 ± 0.42 m w.e.a^{-1} between 2000 and 2015. The mean mass balance of the 9 lacustrine terminating glaciers (–0.70 ± 0.44 m w.e.a^{-1}) we assess was 32 % more negative than land-terminating, debris covered glaciers in our sample. The mass balance of lacustrine-terminating glaciers is highly variable (–0.47 ± 0.35 m w.e. a^{-1} to –0.95 ± 0.52 m w.e. a^{-1}), and we suggest that such a range reflects glacial lakes at different stages of development. Rates of mass loss are therefore likely to increase as glacial lakes expand and calving can occur in deeper water. Hypsometric data reveal a coincidence of the altitude of maximum mass loss and the main glacier hypsometry in the Dudh Koshi catchment, thus a large area of ice is readily available for melt here. Using predicted IPCC AR5 warming scenarios, we assess the effect of temperature increases on current glacier AARs (Dudh Koshi- 0.37, Tama Koshi- 0.36, Tibetan Plateau- 0.40). RCP 4.5 warming (0.9-2.3 ºC by 2100) would reduce these AARs to 0.25 or 0.03 in the Tama Koshi catchment, 0.26 or 0.18 in the Dudh Koshi catchment, and 0.30 or 0.17 on the Tibetan Plateau, respectively. Comparison of our data with a conceptual model of Himalayan glacier shrinkage confirms the presence of three distinct process regimes, with all glaciers in our sample now in a state of accelerating mass loss and meltwater storage. Our results are significant because they suggest that documented glacial lake growth and/or expansion across the Himalaya is likely to be accompanied by increased ice mass loss in the near future. Further, the influence of temperature increases on

glacier AARs may be highly variable across adjacent catchments due to different glacier hypsometry, complicating the prediction of the future contribution of glacial meltwater to river flow.

Keywords: Himalaya, glacier mass, debris-cover, Everest region, glacial lakes

1. Introduction

The Himalaya holds the largest store of glacier ice outside of the polar ice sheets. Estimates of ice volume range from 2,300 km^3 to 7,200 km^3 (Frey et al., 2014 and references within) distributed amongst more than 54,000 glaciers across the Hindu Kush Himalaya (HKH) and the Karakoram (Bajracharya et al., 2015). The current mass balance of Himalayan glaciers is predominantly negative, with accelerating mass loss having been observed over the past few decades (Bolch et al., 2012; Thakuri et al., 2014). This mass loss is occurring because of a combination of processes. Shrestha et al. (1999) show a rise in the mean annual air temperature of 0.057 °C/yr across the Himalaya between 1971 and 1994. Bollasina et al. (2011) show a reduction in total precipitation (–0.95 mm day^{-1}) amounting to 9 to 11% of total monsoon rainfall over a broad area of northern India between 1950 and 1999. Bhutiyana et al. (2010) show both decreasing total precipitation and a changing precipitation phase, with a lower proportion of precipitation falling as snow across the northwest Himalaya between 1996 and 2005. The snow cover season has been shortening as a result (Pepin et al., 2015). Under different climate scenarios, glacier imbalance in the region may contribute 8.7–17.6 mm of sea level rise by 2100 (Huss and Hock, 2015). Prolonged mass loss from Himalayan glaciers may cause diminishing discharge of the largest river systems originating in the region (Immerzeel et al., 2010; Lutz et al., 2014), thereby impacting on Asian water resources in the long-term.

Recent studies have identified spatial heterogeneity in mass loss across the Himalaya in the first decade of the 21st century (Kääb et al., 2012; Gardelle et al., 2013; Kääb et al., 2015). Glaciers in the Eastern Nyainqêntanglha, in the eastern Himalaya, are losing mass most quickly (Kääb et al., 2015), followed by glaciers in the Spiti Lahaul and Hindu Kush (Kääb et al., 2015). Glaciers in the central Himalaya appear to be more stable (Gardelle et al., 2013). The anomalous balanced, or even slightly positive, glacier mass budget in the Karakoram is well documented (Bolch et al., 2012; Gardelle et al., 2012). Few previous studies have assessed the variability of glacier mass loss within catchments (Pellicciotti et al., 2015). Nuimura et al. (2012) examined the altitudinal distribution of glacier surface elevation change in the Khumbu region, Nepal, and found similar surface lowering rates over debris-free and debris-covered glacier surfaces. Gardelle et al. (2013) detected enhanced thinning rates on lacustrine terminating glaciers in Bhutan, West Nepal, and the Everest region, but did not make an explicit comparison with land-terminating glacier recession rates.

Benn et al. (2012) proposed a conceptual model of Himalayan glacier recession that included important thresholds between regimes of ice dynamics and mass loss at different stages of lake development. Benn et al. (2012) also suggested idealised mass balance curves and equilibrium line altitudes (ELAs) that represent each of these regimes and in turn indicate likely future ice loss given sustained climatic forcing. A direct comparison of mass loss data and the model of Benn et al. (2012) is yet to be made, however.

In this work, we aim to quantify glacier mass loss rates in three major catchments of the central Himalaya and assess the glacier-scale variability of ice loss within and between catchments. We specifically examine the mass balance, hypsometry and total area change of each glacier and compare those terminating in a glacial lake with those terminating on land. We use these data together with climatic data from the region to define the major mechanisms that may have driven mass loss in recent decades, and to assess scenarios of likely future ice loss from our sample of glaciers.

2. Study area

We studied glaciers in three catchments of the Everest region (Figure 1), spanning both Nepal and Tibet (China). Two of the catchments, the Dudh Koshi and the Tama Koshi, are located in north-eastern Nepal and drain the southern flank of the Himalaya. The third catchment is located to the north of the divide, and the glaciers drain north into Tibet (China). Most glaciers in the studied catchments are characterised by long (10–15 km), low-slope angle, debris-covered tongues that are flanked by large (tens of metres high) moraine ridges (Hambrey et al., 2008). Some glaciers have accumulation areas several kilometres wide, accumulation zones that reach extreme altitudes (up to 8000 m in the case of the Western Cwn of the Khumbu), whereas others sit beneath mountain massifs (e.g. Lhotse and the Lhotse face), are fed almost exclusively by avalanches and are less than 1 km in width for their entire length.

Of the 278 glaciers in the Dudh Koshi catchment, the largest 40 are partially debris-covered, with debris mantles reaching at least several decimetres in thickness (Rounce and McKinney, 2014; Rowan et al., 2015), and comprise 70 % of the total glacierised area (482 km^2- Bajracharya and Mool, 2009). Here, the total area of glacier surface covered by debris has increased since the 1960s (Thakuri et al., 2014) and several previous studies have published surface lowering data for the catchment indicating accelerating surface lowering rates over recent decades (e.g. Bolch et al., 2011; Nuimura et al. 2012). We select nine of the largest glaciers (Supplementary table 1) for analysis given that they provide the greatest potential volume of meltwater to downstream areas. There are a total of 80 glaciers in the Tama Koshi catchment covering a total area of 110 km^2 (Bajracharya et al., 2015). We again selected the largest nine glaciers (Supplementary table 1) for analysis based

on relative potential contributions to river flow. This is a poorly studied catchment, perhaps best known for the existence of Tsho Rolpa glacial lake, which underwent partial remediation during the 1990s (Reynolds, 1999). The fourteen glaciers within our sample that flow onto the Tibetan Plateau (Supplementary table 1) all contribute meltwater to the Pumqu river catchment, which covers an area of 545 km^2 (Che et al., 2014). Debris cover is less prevalent on glaciers of the Pumqu catchment, and terminus recession has caused a 21 % of glacier area loss since 1970 (Jin et al., 2005; Che et al., 2014). There is relatively little information on glacier ELAs other than in the Dudh Koshi catchment. In the Dudh Koshi, Asahi et al. (2001) estimated ELAs to be at around 5600 m a.s.l. in the early 2000s. Wagnon et al. (2013) measured annually variable ELAs of 5430- 5800 m a.s.l. on the Mera and Polkalde glaciers between 2007 and 2012, Shea et al. (2015) estimate the current ELA to be 5500 m a.s.l., and Gardelle et al. (2013) estimated the ELA to be around 5840 m over the period 2000-2009. On the Tibetan Plateau, those in the Rongbuk catchment were estimated between 5800 and 6200 m a.s.l. for the period 1974-2006 (Ye et al., 2015).

Gardelle et al. (2011) identified 583 supraglacial ponds and lakes in the Everest region. Some of the largest glacial lakes in this region have been expanding in recent decades (Sakai et al., 2000; Che et al., 2014; Somos-Valenzuela et al., 2014). This increased meltwater ponding at glacier termini has potential to affect ice dynamics and down-valley meltwater and sediment fluxes (Carrivick and Tweed, 2013) as well as causing a hazard to populations living downstream. Several of the lakes have burst through their moraine dams in previous decades causing rapid and extensive flooding downstream; the best studied outburst floods are those from Nare glacier in 1977 (Buchroithner et al., 1982) and from Dig Tsho in 1985 (Vuichard and Zimmerman, 1987).

We classify nine glaciers from the sample as lacustrine terminating, where the glacier termini and glacial lakes are actively linked. While both the Gyabrag and Rongbuk glaciers are associated with a proglacial lake we do not consider either as lacustrine terminating. In the case of the Gyabrag Glacier the ice is now separated from the lake by a large outwash plain. In the case of the Rongbuk Glacier, the lake is supraglacial and far up-glacier from its terminal region and thus does not currently influence the recession of the terminus of the glacier. The expanding Spillway Lake at the terminus of Ngozumpa Glacier (Thompson et al., 2012) is currently of limited depth, and is unlikely to affect glacier dynamics in its current state so we also exclude the Ngozumpa from the lacustrine terminating category.

3. Data sources and methods

3.1 Data sources

3.1.1 Digital elevation models

Our reference elevation dataset across all three catchments is the Shuttle Radar Topographic Mission (hereafter SRTM) version 3.0, non-void filled, 1 arc second digital elevation model (hereafter DEM). This dataset was acquired in February 2000 and was released at 30 m resolution in late 2014 (USGS, 2016). SRTM employed two SAR systems, a 5.6 cm C-band (which collected the data we use) and a 3.1 cm X-band system, with the main objective of obtaining single-pass interferometric SAR imagery to be used for DEM generation on a near global scale (56˚S to 60˚ N- 80% of the planet's surface) with targeted horizontal and vertical accuracies of 16 m and 20 m, respectively. Farr et al. (2007) report horizontal and vertical accuracies of better than 10 m for most regions globally.

Our 2014/2015 elevation dataset comprises a number of high resolution (8 m grid) DEMs generated by Ohio State University and distributed online by the Polar Geospatial Centre at the University of Minnesota that provide coverage of an extended area around the Everest region (Table 1). These stereo-photogrammetric DEMs have been generated using a Surface Extraction with TIN-based Search-space Minimization (hereafter SETSM) algorithm from Worldview 1, 2 and 3 imagery (Noh and Howat, 2015). The SETSM algorithm is designed to automatically extract a stereo-photogrammetric DEM from image pairs using only the Rational Polynomial Coefficients (RPCs) as geometric constraints. The geolocation accuracy of RPCs without ground control for Worldview 1 and 2 data is 5 m (Noh and Howat, 2015) which may ultimately result in matching failure. The SETSM algorithm updates RPCs to mitigate this error and produces DEMs with an accuracy of ± 4 m in X, Y and Z directions (Noh and Howat, 2015). SETSM DEMs are gap-filled using a natural neighbour interpolation; we removed these pixels before DEM differencing and the calculation of mass loss rates across the ablation areas of individual glaciers.

Over two small areas of the Dudh Koshi (over the lower reaches of the Bhote Kosi and Melung glaciers) the SETSM DEMs contained data gaps. To complete coverage of DEMs over these glaciers we generated ASTER DEMs and used the surface to cover elevation bands across these glaciers where no data were available from the SETSM grids. We used ERDAS Imagine (2013) to generate ASTER DEMs with ground control points (GCPs) matched between features in the ASTER imagery and the high resolution imagery available in Google Earth. We used a large number of GCPs (45) and tie points (> 75) to minimise the root mean squared (RMS) error of GCP positions. All SETSM and ASTER DEMs were resampled to a 30 m resolution to match that of the SRTM data before any differencing was carried out.

3.1.2 Glacier outlines

Glacier outlines were downloaded from the Global Land Ice Measurement form Space (GLIMS) Randolph Glacier Inventory (RGI) Version 5.0 (Liu and Guo, 2014; Bajracharya et al., 2014; Racoviteanu and Bajracharya, 2008) and modified for 2000 and 2014 glacier extents based on Landsat scenes closely coinciding in acquisition with the DEM data. Glacier extents from these two epochs were used to calculate area changes. The 2000 Landsat scene was acquired by the ETM+ sensor and thus has a single 15 m resolution panchromatic band and six 30 m multispectral bands. The 2014 scene was acquired by the OLI sensor and also has a single 15 m panchromatic band as well as eight 30 m multispectral bands. Both scenes were pan-sharpened to match the resolution of the multispectral bands to that of the panchromatic band before glacier outlines were adjusted. Adjustments were limited to correcting changes in glacier frontal position and changes along the lateral margins because of surface lowering.

3.3 DEM correction

3.3.1 Stereoscopic DEMs

We followed the three-step correction process of Nuth and Kääb (2011), through which biases inherent in stereoscopic DEMs can be corrected. We assessed and corrected where necessary for: (i) mismatch in the geo-location of the modern DEMs versus the reference SRTM dataset (in x, y, and z direction); (ii) the existence of an elevation dependant bias, and; (iii) biases related to the acquisition geometry of the data. Each step was taken individually, so that separate error terms could be understood, rather than bundling them together as multiple regression based adjustments as previous studies have done, such as Racoviteanu et al. (2008) and Peduzzi et al (2010), for example. Corrections applied to DEMs where any one of the three biases were present included shifting of DEM corner coordinates, simple vertical shifting through addition or subtraction, and the fitting of linear and polynomial trends depending on the spatial variability of elevation differences across DEMs and through their elevation ranges. Acquisition geometry related biases (along or cross satellite track) were detected in two SETSM strips (Table 3) and both ASTER scenes and were corrected for using linear trends fitted through difference data. The co-registered DEMs were differenced to yield surface elevation change and outlying values greater than ± 60 m were filtered from the resulting data. DEM co-registration was carried out following the conversion of SETSM elevation data to geoid heights using the Earth Gravitational Model (EGM) 2008 grid available from the National Geospatial-Intelligence Agency.

3.3.2 SRTM DEM correction

Some studies have shown that the SRTM dataset may underestimate glacier surface elevations because of C-band radar wave penetration into snow and ice (Rignot et al., 2001). Kääb et al. (2012) assessed the magnitude of C-band penetration over various test sites in the Himalaya and over different ice facies (clean ice, snow and firn) by extrapolating ICESat Vs SRTM glacier elevation differences back to the SRTM acquisition date, showing penetration estimates of several metres. To account for this bias, we have corrected the SRTM dataset using the penetration estimates of Kääb et al. (2012), after generating a mask for clean ice, firn and snow cover using the most suitable Landsat ETM+ scenes (Table 1) available around the acquisition date of the SRTM dataset. We applied a correction to the SRTM DEM of +4.8 m over areas of firn/snow, and +1.2 m over areas of clean ice (see supplementary table S2 of Kääb et al. (2012)).

Berthier et al. (2006) suggested that the extreme topography present in mountain regions is poorly replicated in coarse-resolution DEMs such as the SRTM DEM. Different studies have applied positive or negative corrections to the SRTM DEM (Berthier et al., 2007; Larsen et al., 2007), depending on the severity of the terrain at their respective study sites. Inspection of DEM differences across the study site showed no clear relationship between elevation differences and altitude (see supplementary information), thus no elevation dependant correction was applied.

3.4 DEM differencing uncertainty

We have assessed three potential sources of error in our surface elevation change data and follow the approach of Wang and Kääb (2015) to estimate the uncertainty associated with elevation changes. We have used the SRTM DEM as our reference dataset and co-registered the SETSM DEMs to it using off-glacier terrain. The absolute height error of the SRTM DEM may be as low as 6.2 m for parts of Eurasia (Farr et al., 2007), but is likely greater over the steep terrain of the Himalaya. We use a value of ± 10 m. According to Wang and Kääb (2015), the absolute accuracy of each DEM (σ_{ab}) can be estimated through:

$$\boldsymbol{\sigma_{ab} = \sqrt{\varepsilon_s^2 + \sigma_i^2}} \quad (1)$$

Where ε_s is the vertical accuracy of the SRTM DEM, and σ_i is the standard error of differences between each SETSM and SRTM DEM. Next, we consider the uncertainty associated with the estimated volume change (σ_{vol}) rate through:

$$\boldsymbol{\sigma_{vol} = 1.96 \text{ x } \frac{\sigma_v'}{\sqrt{N}}} \quad (2)$$

Where σ'_v is the standard deviation of differences multiplied by pixel area. N is the effective number of observations (Bolch et al., 2011). N is calculated through:

$$\boldsymbol{N = \frac{N_{tot} \cdot PS}{2d}} \quad (3)$$

Where N_{tot} is the total number of DEM difference data points, PS is the pixel size and d is the distance of spatial autocorrelation. We follow Bolch et al. (2012) in estimating d to equal 20 pixels.

Finally, we have considered whether the different acquisition dates of Worldview imagery (Table 1) has led to the sampling of seasonal glacier surface elevation variations caused by a remnant snowpack (e.g. Berthier et al. 2016). Such a bias should be partly corrected for during vertical DEM adjustment using off-glacier terrain assuming a similar snowpack thickness on and off-glacier (Wang and Kääb, 2015).

Two overlapping SETSM DEMs (ending FA100 and 3C00 in Table 1) have been generated from Worldview imagery acquired before and after the summer monsoon (when glaciers receive most accumulation) of 2014, thus any spatially consistent off-glacier differences may show a remnant snow pack that would cause an elevation bias. The difference between these two SETSM DEMs is slight (mean -0.17 m, σ 2.84 m), but we cannot be sure that these differences represent a region-wide average. We incorporate an assessment of the standard error (σ_{season}) of these seasonal differences into our overall uncertainty budget:

$$\boldsymbol{\sigma_{season} = \frac{\sigma_{stable}}{\sqrt{N}}} \quad (4)$$

Where σ_{stable} is the standard deviation of stable terrain differences and N is calculated using equation 3 for the FA100-3C00 difference statistics. We summed these three different sources of error quadratically to calculate our overall uncertainty associated with DEM difference data:

$$\boldsymbol{\sigma_{diff} = \sqrt{\sigma_{ab}^2 + \sigma_{vol}^2 + \sigma_{season}^2}} \quad (5)$$

3.5 Hypsometric analysis

Glacier hypsometry, the distribution of glacier area over altitude, is governed by valley shape, relief and ice volume distribution (Jiskoot et al., 2009). It is important for long-term glacier response because it defines the distribution of mass with elevation and thus determines how the glacier responds to changes in elevation-dependent temperature (Furbish and Andrews, 1984). To assess glacier hypsometry, we used the aforementioned glacier outlines and the SETSM DEMs, which offer better data coverage than the non void filled SRTM dataset, to split these glacier extents into segments covering 100 m elevation ranges, and calculated

the area of each segment. We followed the approach of Jiskoot et al. (2009) to categorise each glacier or the population of glaciers in each catchment according to a hypsometric index (HI), where:

$$\boldsymbol{HI} = \frac{(\boldsymbol{H_{max} - H_{med}})}{(\boldsymbol{H_{med} - H_{min}})} \quad (6)$$

and H_{max} and H_{min} are the maximum and minimum elevations of the glacier, and H_{med} the median elevation that divides the glacier area in half (Jiskoot et al., 2009). Glaciers were grouped into five HI categories: 1- HI < –1.5, very top heavy; 2- HI –1.2 to –1.5, top heavy; 3- HI –1.2 to 1.2, equidimensional; 4- HI 1.2 to 1.5, bottom heavy; and 5- HI > 1.5, very bottom heavy. Top heavy glaciers store more ice at higher elevation, for example in broad accumulation zones, whereas bottom heavy glaciers have small accumulation zones and long tongues.

3.6 Mass loss calculations

As in previous mass loss studies in the Himalaya (Bolch et al., 2011; Gardelle et al., 2013) a conversion factor of 900 kg m^{-3} was used to account for the density of glacier ice for all glaciers in the sample. We assigned an additional 7 % to mass loss uncertainty estimates to account for error in the density conversion (Huss, 2013). The mass loss estimates generated for lacustrine terminating glaciers are slight underestimates because, with no information available on bed topography, we cannot account for ice that has been replaced by water during lake expansion. Mass balance estimates for these glaciers therefore only incorporate aerial mass loss from the 2000 calving front, up-glacier. We also acknowledge that our surface lowering estimates incorporate any upward or downward flow of ice resulting from, for example, compressional flow over a zone of transition from active to inactive ice. We do not quantify emergence velocity as the ice thickness and surface velocity data required to do so (Immerzeel et al. 2014) are not available for an adequate number of glaciers in our sample.

3.7 Estimation of ELAs

We follow the method of Nuth et al. (2007) to estimate the ELA of glaciers in our sample. We calculate mean mass balance over 100 m elevation bands for the entire altitudinal range of each glacier, and assume that the altitude at which mass balance curves approach zero is a reliable indicator of the ELA of each glacier over the study period. To estimate prospective future ELAs in response to climatic warming, we used adiabatic lapse rates of –8.5 °C/km for the Tibetan Plateau (Kattel et al., 2015) and –5.4 °C/km for the Dudh Koshi and Tama Koshi catchments (Immerzeel et al., 2014) to calculate prospective ELA shifts given different warming scenarios. We calculated ELAs for projected minimum, mean and maximum temperature increases under the 4 main RCP scenarios outlined in the IPCC AR5 working group report (Collins et al., 2013).

4. Results

4.1 Glacier mass balance

The mean mass balance of all (32) glaciers in our sample was –0.54 ± 0.42 m w.e.a^{-1} between 2000 and 2015. There is considerable variability in the in the mass loss rates of glaciers with different terminus type (Figures 3 and 4) and through the altitudinal range of highlighted glaciers (Figures 5 and 6), but mean mass balance of glaciers in catchments either side of the orographic divide are not markedly different. Mean glacier mass balance (including land and lake terminating glaciers) was –0.51 ± 0.41 m w.e.a^{-1} in the Tama Koshi catchment, –0.60 ± 0.43 m w.e.a^{-1} in the Dudh Koshi catchment, and –0.63 ± 0.41 m w.e.a^{-1} for glaciers flowing onto the Tibetan Plateau over the study period.

The mean mass balance of 9 lacustrine terminating glaciers was –0.70 ± 0.44 m w.e.a^{-1}. This was 32% more negative than land terminating glaciers (mean mass balance of –0.53 ± 0.41 m w.e.a^{-1}) we include in our sample. The lowest mass loss rates occurred over debris-free glaciers at high altitude (5600 – 6200 m a.s.l) on the Tibetan plateau. The mean mass balance of these glaciers was –0.25 ± 0.40 m a^{-1} (supplementary table 2) over the study period.

The altitude at which maximum mass loss rates occurred differed depending on glacier terminus type (Figures 5 and 6). Across all three catchments, substantial mass loss was pervasive over the middle portions of larger, land terminating glaciers (Figure 2). In the Dudh Koshi, mass loss rates are at their highest (–0.86 ± 0.40 m w.e.a^{-1}) around 5200 m a.s.l., although similar surface lowering rates occurred between 5100 and 5300 m a.s.l (Figure 5). In the Tama Koshi the highest rates mass loss (–1.08 ± 0.44 m w.e.a^{-1}) occurred at around 5300 m a.s.l (Figure 5). On the Tibetan Plateau, the highest mass loss rates were almost double those of the Tama Koshi or Dudh Koshi catchments. Between 5300 and 5400 m a.s.l., the mean mass loss rate was –1.96 ± 0.40 m w.e.a^{-1} over the study period. Mass loss rates over glaciers on the Tibetan Plateau were higher than those in the Tama and Dudh Koshi catchments (Figure 5) up to 5700 m a.s.l. (–1.19 ± 0.40 m a^{-1} at this altitude). Of note is the mass loss over clean ice areas high up on glaciers such as the Ngozumpa, Rongbuk, Gyabrag and Bhote Kosi (Figure 2). Surface lowering extended into tributary branches and the cirques of these largest glaciers. Individual glaciers showed much greater mass loss, particularly on the Tibetan Plateau. The Gyabrag glacier lost an exceptional –3.33 ± 0.35 m w.e.a^{-1} between 5300 and 5400 m a.s.l (Figure 5).

The maximum mass loss rates (–2.36 ± 0.44 m w.e.a^{-1}) occurred at the lowest elevations (between 4700 and 4900) of lacustrine terminating glaciers (Figure 6). These 9 glaciers all showed a linear ablation gradient. We

calculate the ablation gradient as the water equivalent of ice melt per 100 m (m w.e.a^{-1}/100 m) vertical elevation change below the ELA. Lacustrine terminating glaciers showed an ablation gradient of 0.57 m w.e.a^{-1}/100 m over the study period. The ablation gradient of land terminating glaciers was non-linear. Surface lowering was negligible around the terminus of most land terminating glaciers, with enhanced ice loss occurring further up-glacier where debris cover may have been thin or patchy. Ablation gradients for the area of land terminating glaciers between the ELA and the altitude of maximum ice loss were 0.49, 0.72 and 0.52 m w.e.a^{-1}/100 m for glaciers on the Tibetan Plateau, and in the Dudh Koshi and Tama Koshi catchments, respectively. Clean ice glaciers also showed a linear ablation gradient- 0.77 m w.e.a^{-1}/100 m. Individual glacier mass balance estimates can be found in the supplementary information.

4.2 Glacier area changes and hypsometry

4.2.1 Total area changes

Two different patterns of ice area loss occurred over the study area during the last 15 years. Lacustrine terminating glaciers and clean ice glaciers all lost ice around their termini/ calving fronts (Figures 3 and 4) as glacial lakes expanded and termini retreated. On average, lacustrine terminating glaciers each lost 0.54 km^2 of ice (3.58% of their total area) over the 15 year study period. Drogpa Nagtsang reduced in size by 2.37 km^2 (9.12 % of its total area: Supplementary Table 3) as the associated rapidly-forming lake expanded. Clean ice glaciers lost 0.09 km^2 of ice (1.31 % of their total area) on average.

Land terminating glaciers lost little area as their surfaces lowered rather than their termini retreating. In the Tama Koshi and Dudh Koshi catchments, and on the Tibetan Plateau, land terminating glaciers lost a mean of 0.14 km^2 (0.50 % of their total area), 0.09 km^2 (0.60 % of their total area) and 0.41 (1.77 % of their total area) of ice, respectively. Over these glaciers, any ice area loss was concentrated up-glacier, where their lateral margins dropped down inner moraine slopes and glacier tongues narrowed slightly.

Overall, our sample of glaciers lost 0.12% of their total area per year over the study period. This figure is identical to that of Bolch et al. (2008) who assessed area change over a smaller number of the same glaciers in our sample between 1962 and 2005. The annual area change rate we calculate is lower than those estimated by Thakuri et al. (2014) and references within. Thakuri et al. (2014) calculated a median annual surface area change rate of –0.42 % a^{-1} in the Dudh Koshi catchment between 1962 and 2011. However, Thakuri et al. (2014) document area change over a number of glaciers that are free of debris cover, and therefore readily advance or retreat in response to climatic change, thus our estimates are not directly comparable.

4.2.2 Glacier hypsometry

The distribution of ice with elevation varies widely among the three studied catchments (Figures 5 and 6). Glaciers of the Dudh Koshi catchment and on the Tibetan Plateau are typically very bottom heavy, with average HI scores of 2.63 and 2.34, respectively (Supplementary Table 1). Glacier hypsometry is concentrated between 4800 and 5500 m (Figure 5) for the Dudh Koshi catchment, and between 5600 and 6500 m on the Tibetan Plateau. Notable exceptions are the Khumbu and Ngozumpa Glaciers which store ice in broad accumulations zones above 7000 m (Supplementary Tables 1 and 2). The majority of glaciers in the Tama Koshi have an equi-dimensional hypsometry (mean HI of 1.14), with most ice stored between 5300 and 5800 m. Glaciers in the Tama Koshi have broader accumulation basins than in the Dudh Koshi catchment, and main glacier tongues are formed of multiple, smaller tributaries flowing from higher altitude in a number of cases (Figure 1). The mean hypsometry (Figure 6) of lacustrine terminating glaciers shows no distinctive morphology as the sample is composed of glaciers from all three catchments in the study area.

4.2.3 Approximate equilibrium line altitudes

We estimate the mean ELA of glaciers in the Dudh Koshi and Tama Koshi catchments, and of our selection of glaciers on the Tibetan Plateau to be 5757, 5677, and 6066 m a.s.l., respectively, although, as Figures 5 and 6 show, the ELA can differ by hundreds of metres on individual glaciers within each catchment. Using those ELAs the accumulation area ratio (AAR) (Dyurgerov et al., 2009) can be estimated for each glacier and this is a parameter strongly related to long-term mass balance (König et al., 2014). We have calculated mean AARs of 0.37, 0.36 and 0.40 for glaciers in the Dudh Koshi and Tama Koshi catchments, and on the Tibetan Plateau, respectively.

5. Discussion

5.1 Variability in rates of ice loss across the orographic divide

The mean mass balance estimates we have derived for glaciers situated in catchments North and South of the orographic divide are not markedly different. However, the contrast in maximum of mass loss from glaciers flowing north of the divide and the sustained mass loss through a broader portion of their elevation range suggests an additional or amplified process has driven glacier change here over recent decades. In this section we discuss possible topographic and climatic drivers of the difference in the rates of mass loss across the range divide.

The Indian summer monsoon delivers extremely large amounts of precipitation (up to 80% of the total annual amount) to the Everest region of Nepal, resulting in high glacier sensitivity to temperature (Fujita, 2008; Sakai et al., 2015). The extreme topography in this region and the location of the orographic divide perpendicular to the prevailing monsoon result in rainfall peaks that are offset from the maximum elevations, with greatest rainfall occurring to the south of the divide and decreasing to the north across the Everest region (Bookhagen and Burbank, 2010; Wagnon et al. 2013). Around 449 mm a^{-1} of rainfall falls at the Pyramid research station (5000 m a.s.l.) at Khumbu Glacier (Salerno et al., 2015), whereas to the north at Dingri on the Tibetan Plateau (4300 m a.s.l.), 263 ± 84.3 mm a^{-1} of rainfall occurs annually (Yang et al., 2011). Snowfall may follow a similar across-range gradient to rainfall, although falling snow may be carried further into the range by prevailing winds from the south. However, no reliable measurements of snowfall exist in this region with which to compare these trends. The north-south precipitation gradient across the orographic divide promotes differences in the response of these glaciers to climate change, such that those to the north are relatively starved of snow accumulation (Owen et al., 2009) and exposed to greater incoming radiative fluxes under generally clearer skies.

During the period of this study (2000–2015), mean annual air temperatures have increased and rainfall amounts appear to have decreased in the Everest region (Salerno et al., 2015). At the Pyramid Observatory at Khumbu Glacier in the Dudh Koshi catchment, increases in minimum (+0.07 °C/a), maximum (+0.009 °C/a) and mean (+0.044 °C/a) annual air temperatures above 5000 m a.s.l. were observed between 1994 and 2013 (Salerno et al., 2015). At Dingri on the Tibetan Plateau 60 km northeast of Mt. Everest, increases in minimum (+0.037 °C/a), maximum (+0.041 °C/a) and mean (+0.037 °C/a) annual air temperatures occurred over the same period (Salerno et al., 2015). Yang et al. (2011) found a clear relationship between increasing temperatures over time at Tingri and at temporary (operational between May 2007 and August 2008) weather stations on the Rongbuk and East Rongbuk glaciers, and suggest that the increases in temperature at Tingri have been replicated at glacierised altitudes. Yang et al. (2011) also show a longer-term increase in the mean annual air temperature at Dingri, as do Shrestha et al. (1999) across the southern flank of the greater Himlaya. Between 1959 and 2007, the mean annual air temperature increased by 0.06 °C/a at Dingri (Yang et al., 2011). Shestha et al. (1990) calculated an increase in the mean annual air temperature of 0.057 °C/a between 1971 and 1994 across a number of sites in the greater Himalaya.

The snowline altitude also appears to have increased recently on the southern flank of the Himalaya; Thakuri et al. (2014) showed a rapid ascent of the snow-line altitude in the Dudh Koshi between 1962 and 2011 (albeit through documenting transient snowlines from single scenes acquired at each epoch), and Khadka et al. (2014)

suggest declining snow cover over the winter and spring months in the glacierised altitudinal ranges of the Tama Koshi catchment, between 2000 and 2009; a factor that may influence accumulation rates. Kaspari et al. (2008) showed decreasing accumulation in the East Rongbuk Glacier Col (6518 m a.s.l.) on the northern side of Mount Everest between the 1970s and 2001.

We suggest that the combination of the orographic precipitation gradient and increasing temperatures over the few decades has caused greater mass loss rates from glaciers on the Tibetan Plateau than those glaciers to the south. We also suggest that measured, contemporary increases in air temperature, observations of increasing snowline altitude and declining accumulation are likely to enhance glacier mass loss across the range in future.

5.2 Comparison of mass balance estimates with other studies

Several other studies have generated geodetic mass balance estimates for glaciers of the Everest region over several different time periods. Bolch et al. (2011) measured a mass balance of –0.32 ± 0.08 m w.e.a^{-1} for ten glaciers to the south and west of Mt Everest over the period 1970-2007. Nuimura et al. (2012) calculated a regional mass balance of –0.45 ± 0.25 m w.e.a^{-1} for 97 glaciers across the region over the period 1992-2008. Kaab et al. (2012) estimated a mass balance of –0.39 ± 0.11 m w.e.a^{-1} for a 3˚ x 3˚ cell centred on the Everest region between 2003 and 2008. Gardelle et al. (2013) calculated a slightly less negative mass balance of –0.26 ± 0.13 m w.e.a^{-1} between 1999 and 2011, although the SRTM penetration correction applied by Gardelle et al. (2013) may have caused bias towards less negative mass balance (Barundun et al., (2015). Our results suggest that the mass loss rates measured by Bolch et al. (2012), Nuimura et al. (2012) and Kaab et al. (2012) have been sustained and possibly increased in recent years.

5.3 The influence of glacial lakes on glacier mass balance

Only Nuimura et al. (2012) have directly compared mass loss rates of lacustrine and land terminating glaciers in the study area, showing faster surface lowering rates over Imja and Lumding glaciers in the Dudh Koshi catchment. Our data confirm that lacustrine terminating glaciers can indeed lose ice at a much faster rate than land terminating glaciers. The variability in the mass balance of the 9 lacustrine terminating glaciers (Figure 6) we highlight suggests the fastest mass loss rates occur in the later stages of lake development. Glaciers such as the Yanong and Yanong North, in the Tama Koshi catchment, sit behind large proglacial lakes and have shown extremely high mass loss rates (–3 m w.e.a^{-1} or more over their lower reaches- Figure 6). These glaciers are now relatively small and steep and no longer possess a debris-covered tongue, and so may represent the end-product of debris-covered glacier wastage described by Benn et al. (2012). In contrast, glaciers such as Duiya or

Longmojian, on the Tibetan Plateau, currently have only small lakes at their termini, showed moderate area losses (0.44 and 0.5 km^2, or 4.28 and 2.07 % of total area, respectively) and mass loss rates (–1 to 2 m $w.e.a^{-1}$). Continued thinning of the terminal regions of these glaciers would lead to a reduction in effective pressure, an increase in longitudinal strain and therefore flow acceleration (Benn et al., 2007). The retreat of the calving front up-valley into deeper bed topography may also increase calving rates (Benn et al., 2007), and a combination of both of these processes would lead to enhanced ice loss. Very little surface velocity data exist for lacustrine terminating debris-covered glaciers. Only Quincey et al. (2009) measured high surface velocities (25 m/a^{-1} or more) over the Yanong glacier (their Figure 4, panel D), suggesting it is possible for lacustrine terminating glaciers to become more dynamic in the later stages of lake development in the Himalaya.

5.4 Glacier stagnation

Quincey et al. (2009) identified a number of glaciers in the Everest region that appear to be predominantly stagnant, with large parts of the long, debris covered glacier tongues in the area showing little to no flow. Watson et al. (2016) have documented an increasing number and total area of supraglacial melt ponds over a number of the same glaciers studied by Quincey et al. (2009) in the Dudh Koshi catchment (Khumbu, Ngozumpa, Lhotse, Imja and Ama Dablam), since the early 2000's. Over these glaciers, our data show a very distinctive surface lowering pattern (Figure 2), with localised, heterogenous surface lowering appearing to mirror the distribution of large supraglacial ponds and ponds networks. This ice loss pattern is prevalent on the Erbu, Gyachung, Jiuda, Shalong, and G1 glaciers (Figure 2), and high resolution imagery available on Google Earth shows that these glaciers also have well developed networks of supraglacial ponds. We would therefore suggest that large parts of the biggest glaciers in the Tama Koshi catchment and on the Tibetan Plateau are also stagnant, and may see increasing supraglacial meltwater storage in the future, similar to that documented by Watson et al. (2016).

5.5 Susceptibility of glaciers to future mass loss

5.5.1 ELA ascent in response to warming

The coincidence of maximum surface lowering rates with the altitude of maximum hypsometry in the Dudh Koshi catchment (Figure 5) means a large amount of ice is readily available to sustain mass loss rates here. Sustained and prolonged mass loss may lead to a bi-modal hypsometry here, with the separation of debris covered glacier tongues and their high-elevation accumulation zones a possibility (Rowan et al., 2015; Shea et al., 2015). Surface lowering maxima in the Tama Koshi catchment presently occur at a slightly lower elevation

range than the main hypsometric concentration, and across lower reaches of glacier tongues on the Tibetan Plateau.

Our ELAs are above those estimated by Asahi (2001) for an earlier epoch (see section 2) and similar to those estimated by Gardelle et al. (2013) over a similar study period to ours, suggesting that ELAs have indeed risen over recent decades. We have calculated prospective, future AARs for glaciers in our sample based on ELA rise driven by temperature increases under the four main Representative Concentration Pathways (RCPs) used by the IPCC in its fifth Assessment Report (AR5). Figure 7 shows these AARs, averaged across each catchment, in response to different levels of temperature rise. These predictions are based on published lapse rates (Immerzeel et al., 2014; Kattel et al., 2015) that may be spatially variable and assume no changes in precipitation type or amount, or any variability in the contribution of avalanches to accumulation.

To allow the comparison of our results with similar estimates of other studies (Shea et al., 2015; Rowan et al., 2015), we focus specifically on ELA rise resulting from RCP 4.5 warming (+0.9 ^{o}C to +2.3 ^{o}C by 2100). Such temperature increases would cause a rise in ELA of between 165 and 425 m in the Dudh and Tama Koshi catchments, and between 107 and 270 m of ELA ascent over glaciers on the Tibetan Plateau. A rise in ELAs would most significantly affect the Tama Koshi catchment glaciers, with AARs potentially decreasing to 0.25 and 0.03, respectively. The greater altitudinal range and higher accumulation zones of glaciers in the Dudh Koshi catchment and on the Tibetan Plateau would dampen the effects of a rise in ELA on glacier mass balance. AARs could decrease to 0.26 or 0.18 in the Dudh Koshi and to 0.30 or 0.17 on the Tibetan Plateau. ELA rise in response to this particular warming scenario would mean a 17-51% increase in the total glacierised area below the ELA on the Tibetan Plateau, a 17-30 % increase in the Tama Koshi catchment, and a 14-37% increase in the Dudh Koshi catchment.

5.5.2 Comparison with a conceptual model of glacier wastage

Benn et al. (2012) presented a conceptual model of Himalayan glacier wastage composed of three distinct process regimes each operating given certain climatic states. They suggested that transitions between these three process regimes marked major thresholds in glacier response to climatic forcing. By comparing the results from this study with the conceptual model of Benn et al. (2012), it is possible to identify at which stage of recession our highlighted glaciers, and which processes will drive glacier melt in the near future.

Figure 8 shows a comparison of the mass balance curves we derive for the three major catchments in the study area, along with the 9 lacustrine terminating glaciers, and the conceptual mass balance curves proposed by Benn

et al. (2012). There is a clear resemblance of the mass balance curves generated for land-terminating glaciers in the three catchments of our study area and the mass balance curve of regime 2 outlined by Benn et al. (2012). The ablation gradients shown by lacustrine terminating glaciers are also very similar to regime 3 of Benn et al. (2012). Regime 2 is typified by accelerating ice loss and distributed water storage, and regime 3 is dominated by calving retreat and high amounts of water storage, according to Benn et al. (2012).

The transition of glaciers from regime 2 to regime 3 depends on the margins of a glacier being 'decoupled', specifically when the supply of supraglacial or englacial sediment at a glaciers margin is greater than the sediment transport capacity of meltstreams (Benn et al., 2003), and a large moraine dam is free to develop. The presence of such a moraine dam allows the formation of base level lakes and large scale calving events to occur, which is the main mechanism of ice loss in regime 3 of the Benn et al. (2012) model. Many of the glaciers we highlight possess a large terminal moraine and long, low surface gradient tongues, and thus seem primed for the transition from regime 2 to regime 3. We would expect an increase in mass loss rates of the lacustrine terminating glaciers that we highlight following the transition of glaciers from regime 2 to regime 3.

6 Conclusions

DEM differencing has revealed substantial mass loss from many large, debris-covered glaciers in the central Himalaya over the last 15 years. Geodetic mass balance estimates have been calculated for 32 glaciers across three different catchments around the Everest region. We found similarly negative mass budgets for glaciers flowing onto the southern flank of the Himalaya, in the Tama Koshi and Dudh Koshi catchments, and onto the Tibetan Plateau. Mass balance curves show that the maximum mass loss rate (-1.96 ± 0.40 m w.e.a^{-1} between 5300 and 5400 m.a.s.l.) of glaciers flowing onto the Tibetan Plateau was almost twice that of the maximum mass loss rate of glaciers flowing south of the orographic divide (-0.86 ± 0.40 m w.e.a^{-1} between 5200 and 5300 m a.s.l. in the Dudh Koshi catchment, -1.08 ± 0.44 m w.e.a^{-1} between 5200 and 5300 m a.s.l. in the Tama Koshi catchment), and that glaciers flowing onto the Tibetan Plateau are losing ice over a much broader altitudinal range than their south-flowing counterparts. We suggest that the across-range contrast in annual precipitation total, combined with rising temperatures over recent decades may have caused greater ice loss rates on the north flowing glaciers that we observe.

The mean mass balance of 9 lacustrine terminating glaciers we assessed was -0.70 ± 0.44 m w.e.a^{-1}, 32% more negative than land terminating glaciers (mean mass balance of -0.53 ± 0.41 m w.e.a^{-1}). The mass balance of 9 lake terminating glaciers ranged from -0.95 ± 0.52 m w.e.a^{-1} to -0.47 ± 0.35 m w.e.a^{-1} and we would suggest

that glacial lakes in the region are at different stages of expansion. Accelerating mass loss is likely from several of these lake terminating glaciers whose termini will retreat into deeper lake water.

Should predicted warming occur in the Everest region, the ELA of glaciers will rise and, depending on glacier hypsometry, greater glacier area will be prone to ablation. We show that glaciers of the Tama Koshi catchment will see the greatest reduction in glacier AAR due to their more equidimensional hypsometry and limited more limited elevation range in comparison to glaciers of the Dudh Koshi or Tibetan Plateau. Warming of +0.9 ^{o}C to +2.3 ^{o}C by 2100 (IPCC AR5 working group report RCP 4.5) would decrease glacier AAR to 0.25 or 0.03 in the Tama Koshi catchment, 0.26 or 0.18 in the Dudh Koshi catchment, and 0.30 or 0.17 on the Tibetan Plateau, respectively.

The patterns of mass loss found in this study support a model of glacier wastage proposed by Benn et al. (2012) in which three distinct process regimes operate. All of the debris-covered glaciers that we have highlighted show evidence of the ablation processes in regimes 2 and 3 of the conceptual model of Benn et al. (2012). According to this model, mass loss rates will accelerate in the near future on glaciers that are presently with supraglacial lakes or small proglacial lakes. Lake expansion over deeper bed topography will promote full depth calving and enhance ice loss on these glaciers. Glaciers showing signs of lake development will lose more mass once their surfaces lower to the level of the base of their damming moraine, the drainage of ponded water is inhibited, and calving rates increase. Catchment wide ice mass loss rates will increase particularly rapidly when any rise in ELA coincides with the altitude of maximum surface lowering and the peak glacier hypsometry.

Author contribution

OK, DQ and JC designed the study. OK carried out all data processing and analysis. OK, DQ, JC and AR wrote the paper.

Acknowledgements

SETSM DEMs are available for download from http://www.pgc.umn.edu/elevation. The SRTM dataset is available from https://lta.cr.usgs.gov/SRTM1Arc. EGM2008 gridded data is available from http://earth-info.nga.mil/GandG/wgs84/gravitymod/egm2008/egm08_gis.html. OK is a recipient of a NERC DTP PhD studentship. We are grateful for the comments of Benjamin Robson for his comments on an early version of the paper, and for guidance on the use of SETSM data from Ian Howat.

References

Arendt, A., Echelmeyer, K., Harrison, W., Lingle, C., Zirnheld, S., Valentine, V., Ritchie, B. and Druckenmiller, M.: Updated estimates of glacier volume changes in the western Chugach Mountains, Alaska, and a comparison of regional extrapolation methods, J Geophys Res-Earth, 111 (F3), 2006.

Arendt, A., Bliss, A., Bolch, T., Cogley, J. G., Gardner, A. S., Hagen, J.-O., Hock, R., Huss, M., Kaser, G., Kienholz, C., Pfeffer, W. T., Moholdt, G., Paul, F., Radić, V., Andreassen, L., Bajracharya, S., Barrand, N.E., Beedle, M., Berthier, E., Bhambri, R., Brown, I., Burgess, E., Burgess, D., Cawkwell, F., Chinn, T., Copland, L., Davies, B., De Angelis, H., Dolgova, E., Earl, L., Filbert, K., Forester, R., Fountain, A. G., Frey, H., Giffen, B., Glasser, N. F., Guo, W. Q., Gurney, S., Hagg, W., Hall, D., Haritashya, U. K., Hartmann, G., Helm, C., Herreid, S., Howat, I., Kapustin, G., Khromova, T., König, M., Kohler, J., Kriegel, D., Kutuzov, S., Lavrentiev, I., LeBris, R., Liu, S. Y., Lund, J., Manley, W., Marti, R., Mayer, C., Miles, E. S., Li, X., Menounos, B., Mercer, A., Mölg, N., Mool, P., Nosenko, G., Negrete, A., Nuimura, T., Nuth, C., Pettersson, R., Racoviteanu, A., Ranzi, R., Rastner, P., Rau, F., Raup, B., Rich, J., Rott, H., Sakai, A., Schneider, C., Seliverstov, Y., Sharp, M., Sigurðsson, O., Stokes, C., Way, R. G., Wheate, R., Winsvold, S., Wolken, G., Wyatt, F., Zheltyhina, N. Randolph Glacier Inventory – A Dataset of Global Glacier Outlines: Version 5.0. Global Land Ice Measurements from Space, Boulder Colorado, USA. Digital Media. 2015.

Asahi, K. Inventory and recent variations of glaciers in the eastern Nepal Himalayas. Journal of the Japanese Society of Snow and Ice, 63, 159-169. 2001.

Bajracharya, S. R., Maharjan, S. B., Shrestha, F., Guo, W., Liu, S., Immerzeel, W. & Shrestha, B. The glaciers of the Hindu Kush Himalayas: current status and observed changes from the 1980s to 2010. International Journal of Water Resources Development, 31, 161-173. 2015.

Bajracharya, Samjwal (submitter); Shrestha, Finu; Bajracharya, Samjwal; Maharjan, SB; Guo, Wanqin (analyst(s)). GLIMS Glacier Database. Boulder, CO. National Snow and Ice Data Center. 2014.

Bajracharya, S. R. & Mool, P. Glaciers, glacial lakes and glacial lake outburst floods in the Mount Everest region, Nepal. Annals of Glaciology, 50, 81-86. 2009.

Barundun, M., Huss, M., Sold, L., Farinotti, D., Azisov, E., Salzmann, N., Usubaliev, R., Merkushkin, A. and Hoelzle, M.: Re-analysis of seasonal mass balance at Abramov glacier 1968–2014, Journal of Glaciology, 61(230), 1103–1117, doi:10.3189/2015JoG14J239, 2015.

Benn, D.I., Lehmkuhl, F. Mass balance and equilibrium line altitudes of glaciers in high mountain environments. Quaternary International 65/66, 15–29. 2000.

Benn, D. I., Kirkbride, M.P., Owen, L.A. & Brazier, V. 2003. Glaciated valley landsystems. In: Evans, D.J.A. (Ed.), Glacial Landsystems. Arnold, pp. 372–406.

Benn, D. I., Warren, C. R. & Mottram, R. H. Calving processes and the dynamics of calving glaciers. Earth-Science Reviews, 82, 143-179. 2007.

Benn, D. I., Bolch, T., Hands, K., Gulley, J., Luckman, A., Nicholson, L. I., Quincey, D., Thompson, S., Toumi, R. & Wiseman, S. Response of debris-covered glaciers in the Mount Everest region to recent warming, and implications for outburst flood hazards. Earth-Science Reviews, 114, 156-174. 2012.

Berthier, E., Arnaud, Y., Kumar, R., Ahmad, S., Wagnon, P. & Chevallier, P. Remote sensing estimates of glacier mass balances in the Himachal Pradesh (Western Himalaya, India). Remote Sensing of Environment, 108, 327-338. 2007.

Berthier, E., Arnaud, Y., Vincent, C. & Remy, F. Biases of SRTM in high-mountain areas: Implications for the monitoring of glacier volume changes. Geophysical Research Letters, 33. 2006.

Berthier, E., Scheifer, E., Clarke, G. K. C., Menounos, B. & Remy, F. Contribution of Alaskan glaciers to sea-level rise derived from satellite imagery. Nature Geoscience, 3, 92-95. 2010.

Berthier, E., Cabot, V., Vincent, C. & Six, D. Decedal region-wide and glacier wide mass balances derived from multi-temporal ASTER satellite digital elevation models. Validation over the Mont-Blanc area. Frontiers in Earth Science, 4. Doi 10.3389/feart.2016.00063. 2016.

Bhutiyana, M.R. Kale, V.S. & Pawar, N.J. Climate change and the precipitation variations in the northwestern Himalaya: 1866-2006. International Journal of Climatology, 30, 535-548. 2010.

Bolch, T., Kulkarni, A., Kääb, A., Huggel, C., Paul, F., Cogley, J. G., Frey, H., Kargel, J. S., Fujita, K., Scheel, M., Bajracharya, S. & Stoffel, M. The State and Fate of Himalayan Glaciers. Science, 336, 310-314. 2012.

Bolch, T., Pieczonka, T. & Benn, D. I. Multi-decadal mass loss of glaciers in the Everest area (Nepal Himalaya) derived from stereo imagery. Cryosphere, 5, 349-358. 2011.

Bollasina, M. A., Ming, Y. & Ramaswamy, V. Anthropogenic Aerosols and the Weakening of the South Asian Summer Monsoon. Science, 334, 502-505. 2011.

Bookhagen, B. & Burbank, D. Towards a complete Himalayan hydrologic budget: The spatiotemporal distribution of snow melt and rainfall and their impact on river discharge. Journal of Geophysical Research, 115, p.F03019.

Buchroithner, M. F., Jentsch, G. & Wanivenhaus, B. Monitoring of recent geological events in the Khumbu area (Himalaya, Nepal) by digital processing of landsat MSS data. Rock mechanics, 15, 181-197. 1982.

Carrivick, J. L., & Tweed, F. S. Proglacial lakes: character, behaviour and geological importance. Quaternary Science Reviews, 78, 34-52. 2013.

Che, T., Xaio, L. & Liou, Y.-A. Changes in Glaciers and Glacial Lakes and the Identification of Dangerous Glacial Lakes in the Pumqu River Basin, Xizang (Tibet). Advances in Meteorology, 2014, 8. 2014.

Collins, M., R. Knutti, J. Arblaster, J.-L. Dufresne, T. Fichefet, P. Friedlingstein, X. Gao, W.J. Gutowski, T. Johns, G. Krinner, M. Shongwe, C. Tebaldi, A.J. Weaver and M. Wehner, 2013: Long-term Climate Change: Projections, Commitments and Irreversibility. In: Climate Change 2013: The Physical Science Basis. Contribution of Working Group I to the Fifth Assessment Report of the Intergovernmental Panel on Climate Change [Stocker, T.F., D. Qin, G.-K. Plattner, M. Tignor, S.K. Allen, J. Boschung, A. Nauels, Y. Xia, V. Bex and P.M. Midgley (eds.)]. Cambridge University Press, Cambridge, United Kingdom and New York, NY, USA

Dyurgerov, M., Meier, M. F. & Bahr, D. B. A new index of glacier area change: a tool for glacier monitoring. Journal of Glaciology, 55, 710-716. 2009.

Farr, T.G., Rosen, P.A., Carop, E., Crippen, R., Duren, R., Hensley, S., Korbick, M., Paller, M., Rodriguez, E., Roth, L., Seal, D., Shaffer, S., Shimada, J., Umland, J., Werner, M., Oskin, M., Burbank, D. & Alsdorf, D. The Shuttle Radar Topography Mission. Reviews of Geophysics, 45. doi:10.1029/2005RG000183. 2007.

Frey, H., Machguth, H., Huss, M., Huggel, C., Bajracharya, S., Bolch, T., Kulkarni, A., Linsbauer, A., Salzmann, N. & Stoffel, M. Estimating the volume of glaciers in the Himalayan-Karakoram region using different methods. The Cryosphere, 8, 2313-2333. 2014.

Furbish, D.J. & Andrews, J.T. The use of hypsometry to indicate long term stability and response of valley glaciers to changes in mass transfer. Journal of Glaciology, 30, 105, 199-211.

Fujita, K.: Effect of precipitation seasonality on climatic sensitivity of glacier mass balance, Earth and Planetary Science Letters, 276, 14–19, doi:10.1016/j.epsl.2008.08.028, 2008.

Gardelle, J., Arnaud, Y. & Berthier, E. Contrasted evolution of glacial lakes along the Hindu Kush Himalaya mountain range between 1990 and 2009. Global and Planetary Change, 75, 47-55. 2011.

Gardelle, J., Berthier, E. and Arnaud, Y.: Slight mass gain of Karakorum glaciers in the early 21st century, Nat Geosci, 5(5), 322–325, doi:10.1038/ngeo1450, 2012.

Gardelle, J., Berthier, E., Arnaud, Y. & Kääb, A. Region-wide glacier mass balances over the Pamir-Karakoram-Himalaya during 1999-2011. Cryosphere, 7, 1263-1286. 2013.

Hambrey, M. J., Quincey, D. J., Glasser, N. F., Reynolds, J. M., Richardson, S. J. & Clemmens, S. Sedimentological, geomorphological and dynamic context of debris-mantled glaciers, Mount Everest (Sagarmatha) region, Nepal. Quaternary Science Reviews, 27, 2361-2389. 2008.

Huss, M. & Hock, R. A new model for global glacier change and sea-level rise. Frontiers in Earth Science, 3. 2015.

Immerzeel, W. W., Van Beek, L. P. H. & Bierkens, M. F. P. Climate Change Will Affect the Asian Water Towers. Science, 328, 1382-1385. 2010.

Immerzeel, W.W., Kraaijenbrink, M. Shea, J.M., Shrestha, A.B., Pellicciotti, F., Bierkens, M.F.P. & de Jong, S.M. High-resolution monitoring of Himalayan glacier dynamics using unmanned aerial vehicles. Remote Sensing of Environment, 150, 93-103. 2014.

Jin, R., Li, X., Che, T., WU, L. & Mool, P. Glacier area changes in the Pumqu river basin, Tibetan Plateau, between the 1970s and 2001. Journal of Glaciology, 51, 607-610. 2005.

Jiskoot, H., Curran, C. J., Tessler, D. L. & Shenton, L. R. Changes in Clemenceau Icefield and Chaba Group glaciers, Canada, related to hypsometry, tributary detachment, length, slope and area & aspect relations. Annals of Glaciology, 50, 133-143. 2009.

Kääb, A. Combination of SRTM3 and repeat ASTER data for deriving alpine glacier flow velocities in the Bhutan Himalaya. Remote Sensing of Environment, 94, 463-474. 2005.

Kääb, A., Berthier, E., Nuth, C., Gardelle, J. & Arnaud, Y. Contrasting patterns of early twenty-first-century glacier mass change in the Himalayas. Nature, 488, 495-498. 2012.

Kääb, A., Treichler, D., Nuth, C. and Berthier, E., 2015. Brief Communication: Contending estimates of 2003–2008 glacier mass balance over the Pamir–Karakoram– Himalaya. The Cryosphere, 9(2), pp.557-564. 2015.

Kapnick, S. B., Delworth, T. L., Ashfaq, M., Malyshev, S. & Milly, P. C. D. Snowfall less sensitive to warming in Karakoram than in Himalayas due to a unique seasonal cycle. Nature Geosci, 7, 834-840. 2014.

Kaspari, S., Hooke, R. LeB., Mayewski, P.A., Kang, S.C., Hou, S.G. & Qin, D.H. Snow accumulation rate on Qomolangma (Mount Everest), Himalaya: synchroneity with sites across the Tibetan Plateau on 50-100 year timescales. Journal of Glaciology, 54, 185, 343-352. Doi: 10.3189/002214308784886126. 2008.

Kattel, D. B., Yao, T., Yang, W., Gao, Y. & Tian, L. Comparison of temperature lapse rates from the northern to the southern slopes of the Himalayas. International Journal of Climatology, 35, 4431-4443. 2015.

Khadka, D., Babel, M. S., Shrestha, S. & Tripathi, N. K. Climate change impact on glacier and snow melt and runoff in Tamakoshi basin in the Hindu Kush Himalayan (HKH) region. Journal of Hydrology, 511, 49-60. 2014.

König, M., Nuth, C., Kohler, J., Moholdt, G. & Pettersen, R. A digital glacier database for svalbard. In: Kargel, S. J., Leonard, J. G., Bishop, P. M., Kääb, A. & Raup, H. B. (eds.) Global Land Ice Measurements from Space. Berlin, Heidelberg: Springer Berlin Heidelberg. 2014.

Larsen, C. F., Motyka, R. J., Arendt, A. A., Echelmeyer, K. A. & Geissler, P. E. Glacier changes in southeast Alaska and northwest British Columbia and contribution to sea level rise. Journal of Geophysical Research: Earth Surface, 112, F01007. 2007.

Liu, Shiyin (submitter); Liu, Shiyin; Guo, Wanqin (analyst(s)). GLIMS Glacier Database. Boulder, CO. National Snow and Ice Data Center. 2014.

Lutz, A. F., Immerzeel, W. W., Gobiet, A., Pellicciotti, F. & Bierkens, M. F. P. Comparison of climate change signals in CMIP3 and CMIP5 multi-model ensembles and implications for Central Asian glaciers. Hydrol. Earth Syst. Sci., 17, 3661-3677. 2013.

Melkonian, A.K., Willis, M.J., Pritchard, M.E., Rivera, A., Bown, F. & Bernstein. Satellite-derived volume loss rates and glacier speeds for the Cordillera Darwin Icefield, Chile. The Cryosphere, 7, 823-829. doi:10.5194/tc-7-823-2013. 2013.

Melkonian, A.K., Willis, M.J., Pritchard, M.E. Satellite-derived volume loss rates and glacier speeds for the Juneau Icefield, Alaska. Journal of Glaciology, 60 (222). Doi:10.3189/2014JoG13J181. 2014.

Noh, M. J. & Howat, I. M. Automated stereo-photogrammetric DEM generation at high latitudes: Surface Extraction with TIN-based Search-space Minimization (SETSM) validation and demonstration over glaciated regions. GIScience & Remote Sensing, 52, 198-217. 2015.

Nuimura, T., Fujita, K., Yamaguchi, S. & Sharma, R. R. Elevation changes of glaciers revealed by multitemporal digital elevation models calibrated by GPS survey in the Khumbu region, Nepal Himalaya, 1992-2008. Journal of Glaciology, 58, 648-656. 2012.

Nuth, C. & Kääb, A. Co-registration and bias corrections of satellite elevation data sets for quantifying glacier thickness change. Cryosphere, 5, 271-290. 2011.

Nuth, C., Kohler, J., Aas, H. F., Brandt, O. & Hagen, J. O. Glacier geometry and elevation changes on Svalbard (1936-90): a baseline dataset. In: SHARP, M. (ed.) Annals of Glaciology, Vol 46, 2007. Cambridge: Int Glaciological Soc. 2007.

Owen, L.A. Robinson, R., Benn, D.I., Finkel, R.C., Davis, N.K., Yi, C., Putkonen, J., Li, D. & Murray, A.S. Quaternary glaciation of Mount Everest. *Quaternary Science Reviews*, 28(15-16), pp.1412–1433. 2009.

Pellicciotti, F., Stephan, C., Miles, E., Herreid, S., Immerzeel, W. W. & Bolch, T. Mass-balance changes of the debris-covered glaciers in the Langtang Himal, Nepal, from 1974 to 1999. Journal of Glaciology, 61, 373-386. 2015.

Pepin, N., Bradley, R.S., Diaz, H.F., Baraer, M., Caceres, E.B., Forsythe, N., Fowler, G., Greenwood, M.Z., Hashmi, X.D., Liu, J.R., Miller, K., Ning, A., Ohmura, E., Palazzi, I., Rangwala, W., Schöner, I., Seversky, M., Shahgedanova, M., Wang, S.N. Williamson, N. & Yang, D.Q. Elevation-dependent warming in mountain regions of the world. Nature Clim. Change, 5, 424-430. 2015.

Quincey, D. J., Luckman, A. & Benn, D. Quantification of Everest region glacier velocities between 1992 and 2002, using satellite radar interferometry and feature tracking. Journal of Glaciology, 55, 596-606. 2009.

Quincey, D. J., Richardson, S. D., Luckman, A., Lucas, R. M., Reynolds, J. M., Hambrey, M. J. & Glasser, N. F. Early recognition of glacial lake hazards in the Himalaya using remote sensing datasets. Global and Planetary Change, 56, 137-152. 2007.

Racoviteanu, Adina (submitter); Bajracharya, Samjwal (analyst(s)). GLIMS Glacier Database. Boulder, CO. National Snow and Ice Data Center. 2008.

Rankl, M. & Braun, M.: Glacier elevation and mass changes over the central Karakoram region estimated from TanDEM-X and SRTM/X-SAR digital elevation models, Annals of Glaciology, 51(71), 273–280, doi:10.3189/2016AoG71A 024, 2016.

Reynolds, J.M. Glacial hazard assessment at Tsho Rolpa, Rolwaling, Central Nepal. Quaterly Journal of Engineering Geology and Hydrogeology, 32, 209-214. 1999.

Rignot, E., Echelmeyer, K. & Krabill, W. Penetration depth of interferometric synthetic-aperture radar signals in snow and ice. Geophysical Research Letters, 28, 3501-3504. 2001.

Rounce, D. R. & McKinney, D. C. Debris thickness of glaciers in the Everest area (Nepal Himalaya) derived from satellite imagery using a nonlinear energy balance model. The Cryosphere, 8, 1317-1329. 2014.

Rowan, A. V., Egholm, D. L., Quincey, D. J. & Glasser, N. F. Modelling the feedbacks between mass balance, ice flow and debris transport to predict the response to climate change of debris-covered glaciers in the Himalaya. Earth and Planetary Science Letters, 430, 427-438. 2015.

Rupper, S., Schaefer, J.M., Burgener, L.K., Koenig, L.S., Tsering, K. & Cook, E.R. Sensitivity and response of Bhutanese glaciers to atmospheric warming. *Geophysical Research Letters*, 39(19), p.L19503. 2012.

Sakai, A., Chikita, K. & Yamada, T. Expansion of a moraine-dammed glacial lake, Tsho Rolpa, in Rolwaling Himal, Nepal Himalaya. Limnology and Oceanography, 45, 1401-1408. 2000.

Sakai, A., Nuimura, T., Fujita, K., Takenaka, S., Nagai, H. and Lamsal, D.: Climate regime of Asian glaciers revealed by GAMDAM glacier inventory, The Cryosphere, 9(3), 865–880, doi:10.5194/tc-9-865-2015, 2015.

Salerno, F., Guyennon, N., Thakuri, S., Viviano, G., Romano, E., Vuillermoz, E., Cristofanelli, P., Stocchi, P., Agrillo, G., Ma, Y. & Tartari, G. Weak precipitation, warm winters and springs impact glaciers of south slopes of Mt. Everest (central Himalaya) in the last 2 decades (1994–2013). The Cryosphere, 9, 1229-1247. 2015.

Shea, J.M., Immerzeel, W.W., Wagnon, P., Vincent, C. and Bajracharya, S. Modelling glacier change in the Everest region, Nepal Himalaya. The Cryosphere, 9(3), pp.1105-1128. 2015.

Shrestha, A. B., Wake, C. P., Mayewski, P. A. & Dibb, J. E. Maximum temperature trends in the Himalaya and its vicinity: An analysis based on temperature records from Nepal for the period 1971-94. Journal of Climate, 12, 2775-2786. 1999.

Somos-Valenzuela, M. A., Mckinney, D. C., Rounce, D. R. & Byers, A. C. Changes in Imja Tsho in the Mount Everest region of Nepal. Cryosphere, 8, 1661-1671. 2014.

Thakuri, S., Salerno, F., Smiraglia, C., Bolch, T., D'Agata, C., Viviano, G. & Tartari, G. Tracing glacier changes since the 1960s on the south slope of Mt. Everest (central Southern Himalaya) using optical satellite imagery. Cryosphere, 8, 1297-1315. 2014.

USGS. 2016. *Shuttle Radar Topography Mission (SRTM) 1 Arc-Second Global*. [ONLINE] Available at: https://lta.cr.usgs.gov/SRTM1Arc. [Accessed 08 March 2016]

Vuichard, D. & Zimmerman, M. The 1985 Catastrophic Drainage of a Moraine-Dammed Lake, Khumbu Himal, Nepal: Cause and Consequences. Mountain Research and Development, 7, 91-110. 1987.

Wagnon, P., Vincent, C., Arnaud, Y., Berthier, E., Vuillermoz, E., Gruber, S., Ménégoz, M., Gilbert, A., Dumont, M., Shea, J.M. and Stumm, D. Seasonal and annual mass balances of Mera and Pokalde glaciers (Nepal Himalaya) since 2007. Cryosphere, 7(6), pp.1769-1786. 2013.

Watson, C.S. Quincey, D.J, Carrivick, J.L. and Smith, M.W. The dynamics of supraglacial ponds in the Everest region, central Himalaya. Global and Planetary Change, 142, 14-27. 2016.

Yang, X., Zhang, T., Qin, D., Kang, S. & Qin, X. Characteristics and Changes in Air Temperature and Glacier's Response on the North Slope of Mt. Qomolangma (Mt. Everest). Arctic, Antarctic, and Alpine Research, 43, 147-160. 2011.

Ye, Q., Bolch, T., Naruse, R., Wang, Y., Zong, J., Wang, Z., Zhao, R., Yang, D. & Kang, S. Glacier mass changes in Rongbuk catchment on Mt. Qomolangma from 1974 to 2006 based on topographic maps and ALOS PRISM data. Journal of Hydrology, 530, 273-280. 2015.

Table 1. Scenes used in glacier outline delineation, ASTER DEM generation, SRTM ice facies mask generation and by the Polar Geospatial Centre in the generation of SETSM DEMs.

Sensor	Scene ID	Date of acquisition	Purpose
Landsat OLI	LC81400412014334LGN00	30/11/2014	Glacier outlines
Landsat ETM+	LE71390412000302SGS00	29/10/2000	Glacier outlines
Landsat ETM+	LE71400402002005SGS00	05/01/2002	Ice facies mask
Landsat ETM+	LE71400412002005SGS00	05/01/2002	Ice facies mask
ASTER	L1A.003:2014050545	29/11/2014	ASTER DEM
ASTER	L1A.003:2014045939	12/04/2014	ASTER DEM
Worldview 3	WV03_20150121_10400100076C0700	21/01/2015	SETSM DEM
Worldview 1	WV01_20150504_102001003C5FB900	04/05/2015	SETSM DEM
Worldview 1	WV01_20140115_102001002A289F00	15/01/2014	SETSM DEM
Worldview 2	WV02_20140311_103001002E546F00	11/03/2014	SETSM DEM
Worldview 1	WV01_20140324_102001002D263400	24/03/2014	SETSM DEM
Worldview 1	WV01_20150204_102001003A5B7900	04/02/2015	SETSM DEM
Worldview 2	WV02_20150202_103001003D4C7900	02/02/2015	SETSM DEM
Worldview 1	WV01_20140218_102001002C5FA100	18/02/2014	SETSM DEM
Worldview 1	WV01_20141022_102001003525D400	22/10/2014	SETSM DEM
Worldview 1	WV01_20150131_1020010038618500	31/01/2015	SETSM DEM
Worldview 2	WV02_20141226_103001001D66C000	26/12/2014	SETSM DEM
Worldview 2	WV02_20141110_1030010039013C00	10/11/2014	SETSM DEM
Worldview 1	WV01_20141129_102001002776B500	29/11/2014	SETSM DEM
Worldview 1	WV01_20140514_102001003001E400	14/05/2014	SETSM DEM

Table 2. Mean differences and the standard deviation associated with off-glacier elevation difference data between ASTER, SETSM and SRTM DEMs before and after the DEM correction process. The uncertainty associated with DEM difference data is also listed for each SETSM and ASTER DEM.

Sensor	ASTER scene ID	Pre correction mean & StDev stable ground differences Vs SRTM (m)		Post correction mean & StDev stable ground differences Vs SRTM (m)		dh/dt uncertainty (± m a^{-1})
ASTER	L1A.003:2014050545	–64.12	25.99	0.43	11.30	0.87
	SETSM tile					
WV 3	WV03_20150121_10400100076C0700	–37.37	11.44	0.53	6.43	0.38
WV 1	WV01_20150504_102001003C5FB900	–30.77	14.11	–0.43	5.89	0.32
WV 1	WV01_20140115_102001002A289F00	–32.76	7.41	0.50	6.64	0.49
WV 2	WV02_20140311_103001002E546F00	–24.13	15.57	–0.13	6.06	0.49
WV 1	WV01_20140324_102001002D263400	–30.84	8.56	0.07	5.90	0.38
WV 1	WV01_20150204_102001003A5B7900	–34.28	18.09	–0.36	5.65	0.47
WV 2	WV02_20150202_103001003D4C7900	–34.00	12.81	–0.03	6.56	0.38
WV 1	WV01_20140218_102001002C5FA100	–32.16	9.78	–0.23	6.71	0.52
WV 1	WV01_20141022_102001003525D400	–30.88	14.81	0.36	6.89	0.49
WV 1	WV01_20150131_1020010038618500	–28.99	22.87	–0.83	5.70	0.41
WV 2	WV02_20141110_1030010039013C00	–26.61	7.70	0.07,	5.87	0.45
WV 1	WV01_20141129_102001002776B500	–34.06	6.05	0.16	4.76	0.32
WV 1	WV01_20140514_102001003001E400	–32.33	9.17	–0.26	5.91	0.39

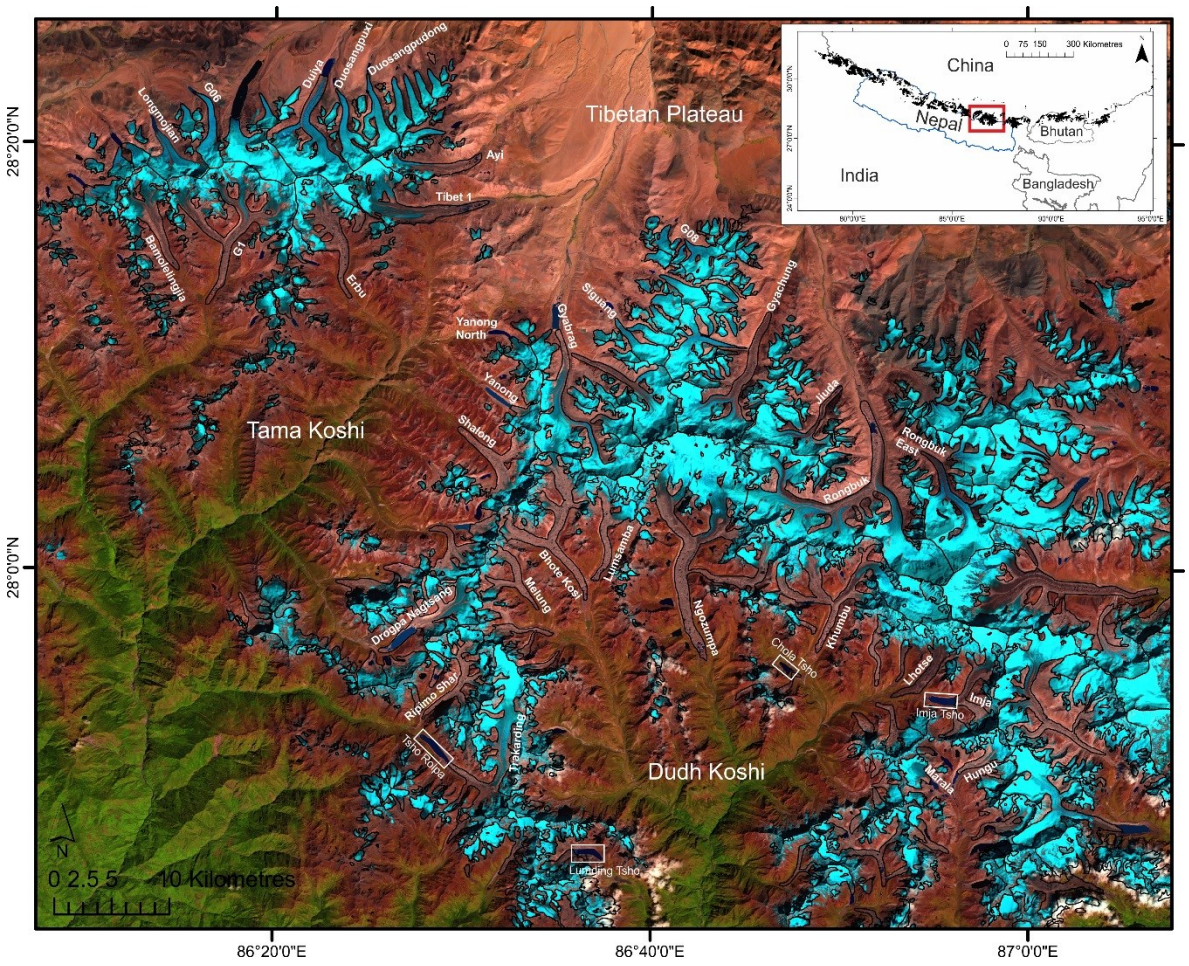

Figure 1. The glaciers of the Everest region. Named glaciers are the glaciers we highlight in this study. Major catchments include the Tama Koshi and Dudh Koshi on the southern flank of the Himalaya and the Pumqu river catchment on the northern side of the divide, with glaciers flowing onto the Tibetan Plateau (China). Named glacial lakes are highlighted, although many remain unnamed. Background imagery is a Landsat OLI image from 2014 available from http://earthexplorer.usgs.gov/.

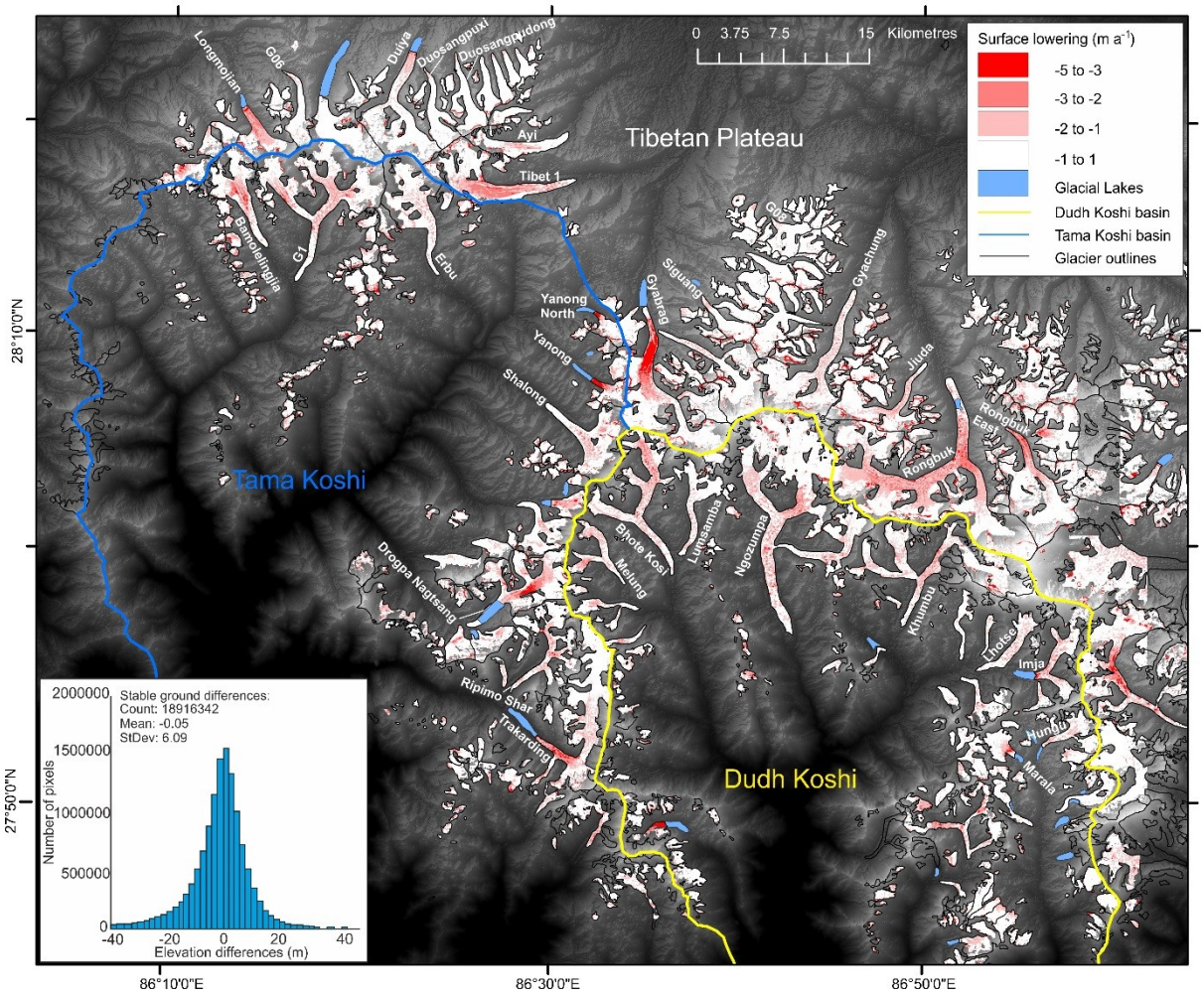

Figure 2. Glacier surface lowering over the study area between 2000 and 2014/15. Also shown is a summary of off-glacier terrain differences.

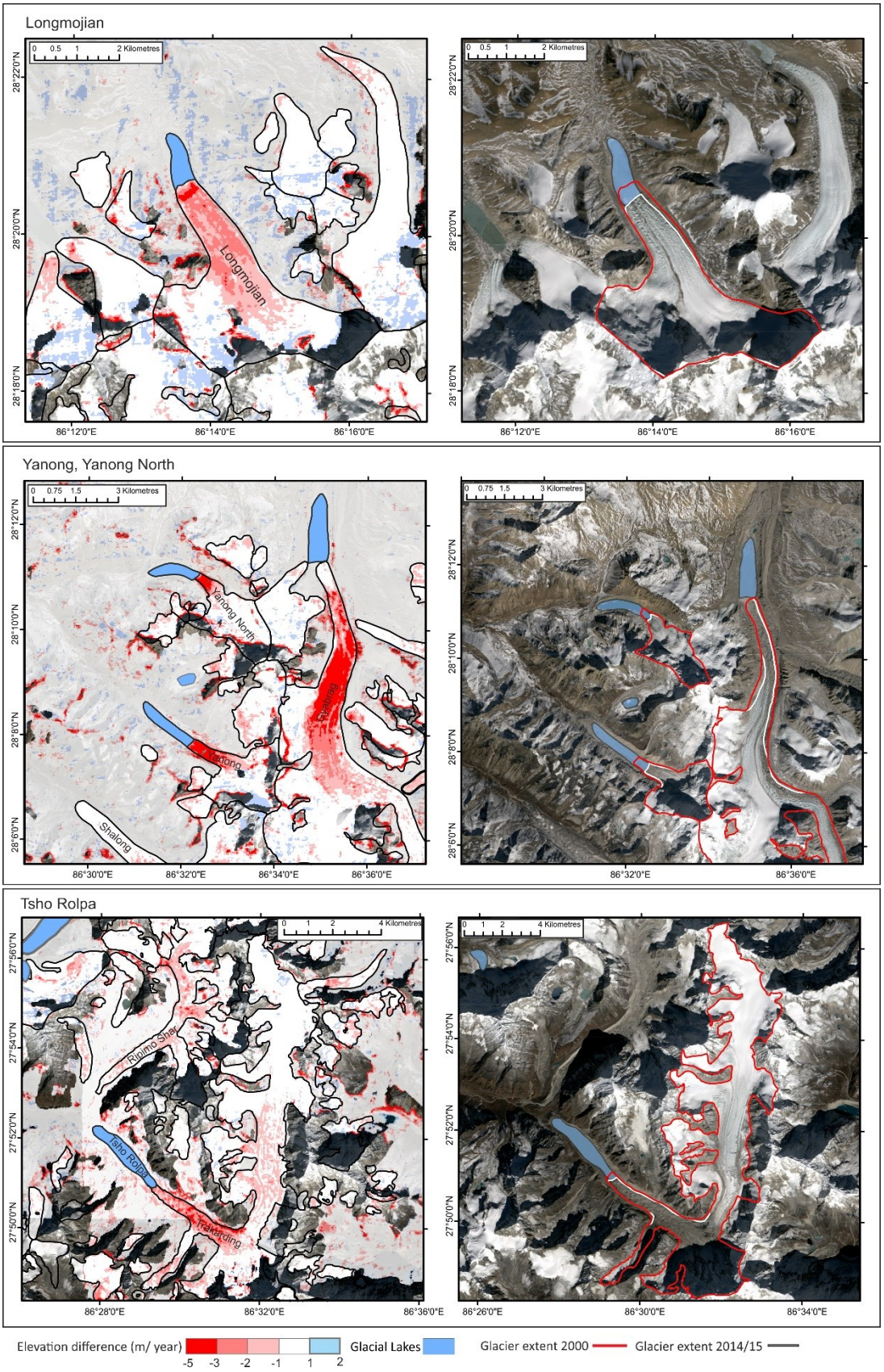

Figure 3. Examples of surface lowering and total area change over the study period on lacustrine terminating glaciers. Semi-transparent, off-glacier differences are also shown.

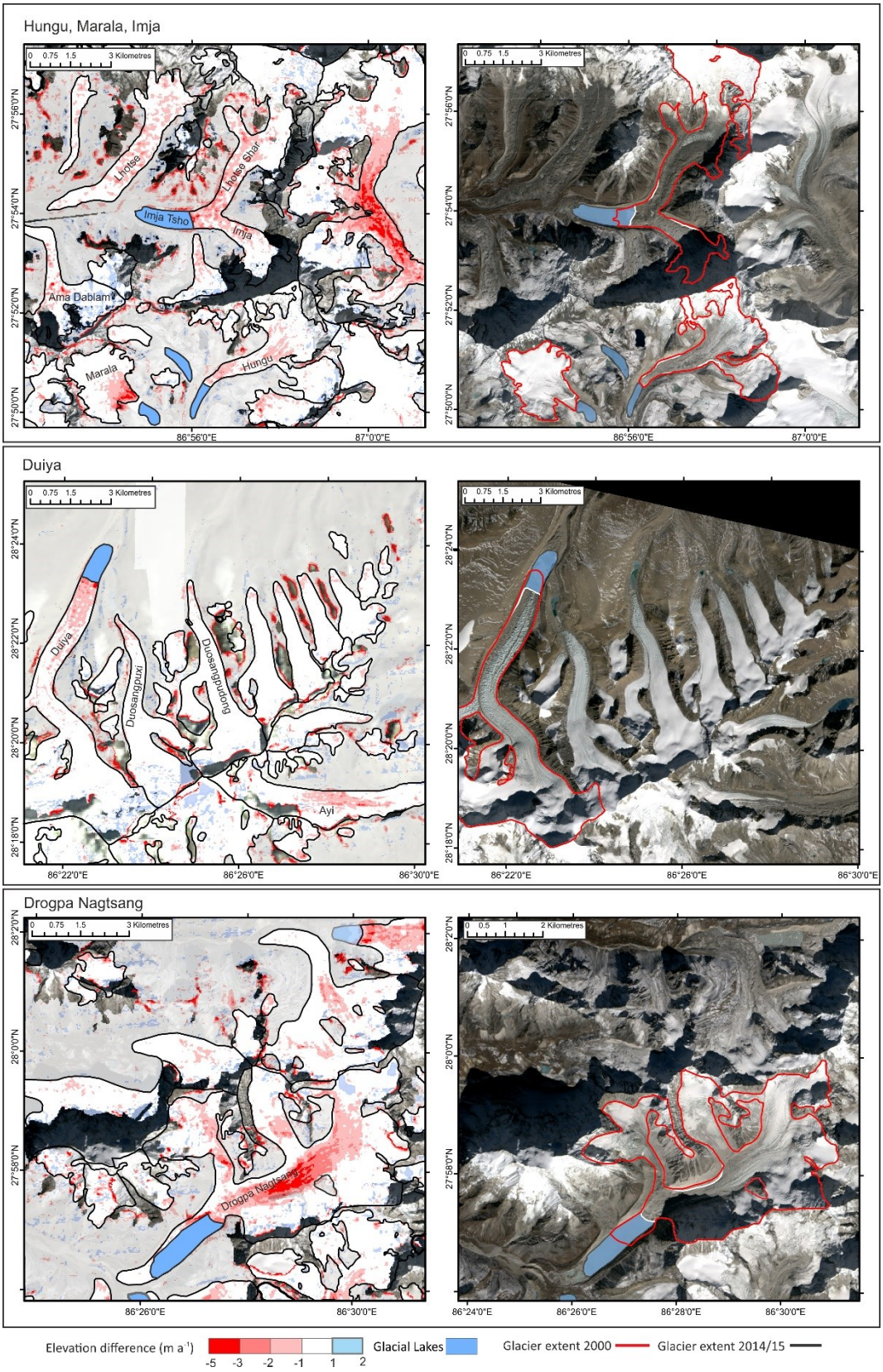

Figure 4. Further examples of surface lowering and total area change over the study period on lacustrine terminating glaciers. Semi-transparent, off-glacier differences are also shown.

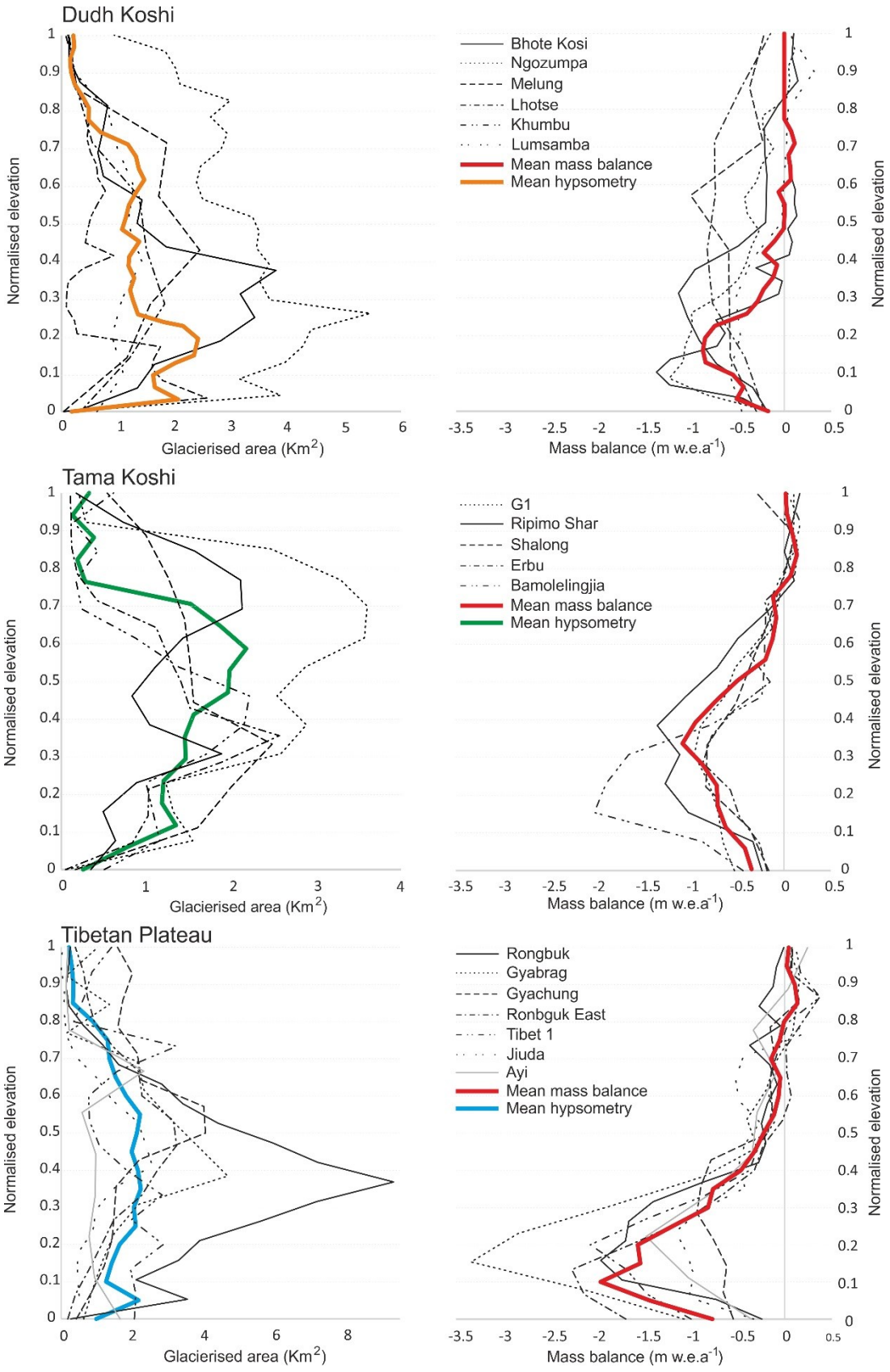

Figure 5. Mass balance and glacier hypsometry curves for all land terminating glaciers in the three different catchments of the study area.

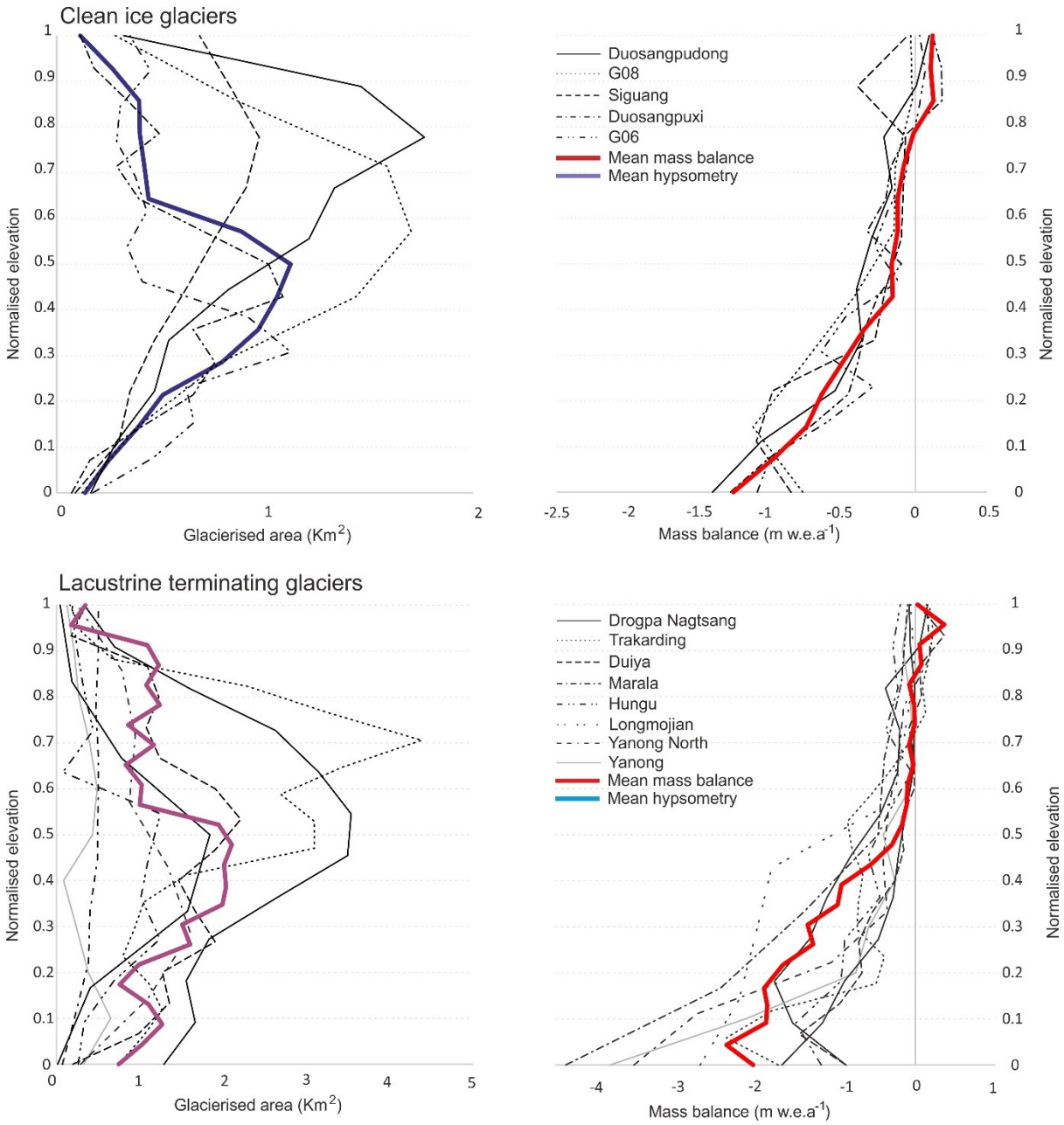

Figure 6. Mass balance and glacier hypsometry curves for clean ice and lacustrine terminating glaciers in the study area.

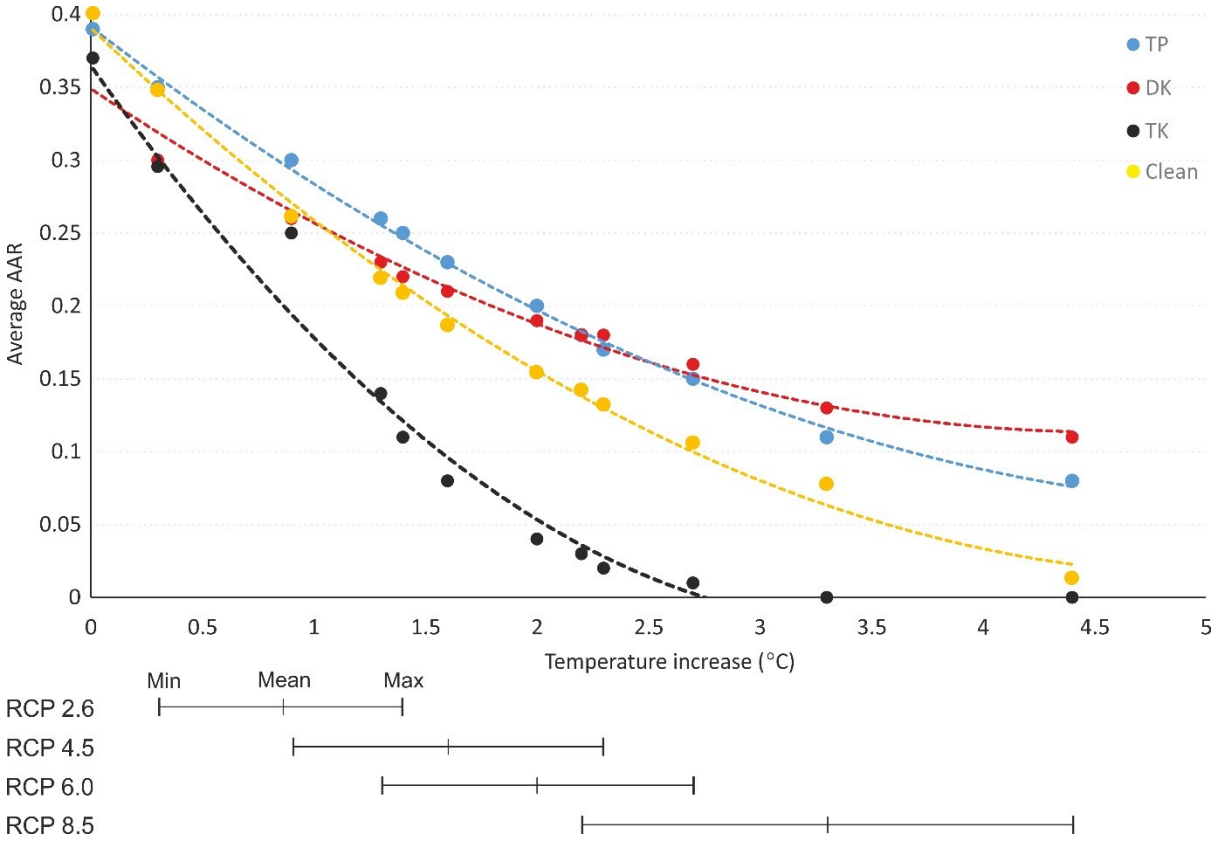

Figure 7. Projected AARs (averaged across each catchment) based on different scenarios of temperature increase relative to the present day and accompanying ELA rise. Temperature rise scenarios have been used from the IPCC AR5 Working Group report. TP- Tibetan Plateau; DK- Dudh Koshi; TK- Tama Koshi; Clean- Clean ice glaciers.

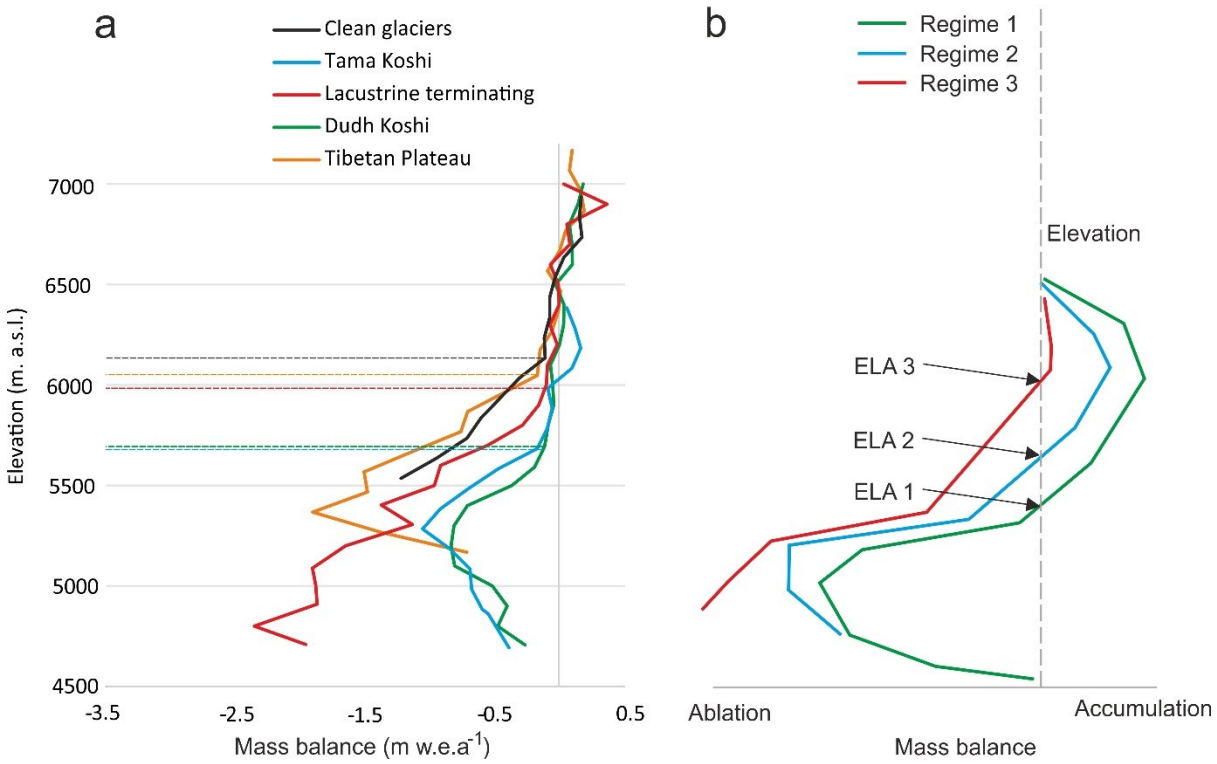

Figure 8. A- Mass balance curves for land terminating glaciers averaged across each catchment and for the populations of clean ice and lacustrine terminating glaciers we highlight. ELAs estimated from the altitude at which mass balance curves approach zero are marked by dashed lines in matching colours. B- Mass balance curves proposed by Benn et al. (2012) to represent three distinct regimes of ice melt on debris-covered glaciers.